JOURNAL OF AIRCRAFT
Vol. 29, No. 6, Nov.–Dec. 1992

Optimized Scramjet Integration on a Waverider

Mary Kae L. O'Neill* and Mark J. Lewis†
University of Maryland, College Park, Maryland 20742

Scramjet integrated waverider airframes optimized for maximum thrust margin and lift-to-drag ratio (L/D) are presented. Parameters affecting the success of the scramjet/waverider system are reviewed and the computer code developed to optimize the integrated system is discussed. In this study, conically derived waveriders are specifically designed to supply the scramjet engines with the required properties for effective combustion. The results of this study show that the waverider airframe lends itself well to scramjet engine integration, yielding promising vehicle configurations.

Nomenclature

D	=	drag
Isp	=	specific impulse
L	=	lift
M	=	Mach number
T	=	thrust
$(T - D)/D$	=	thrust margin
β	=	conical shock angle, deg
γ	=	ratio of specific heats

Introduction

ONE of the keys to the success of an airbreathing hypersonic vehicle is the effective integration of the air-breathing engine with the airframe. To reduce overall drag and achieve positive thrust margins at hypersonic velocities, the engine must be made an integral part of the airframe. The engine and airframe aerodynamics therefore become highly coupled. The forebody becomes the precompression surface, thereby supplying the engine flowfield, and the aftbody becomes the nozzle.

The waverider airframe configuration has been shown both computationally[1,2] and experimentally[3] to yield higher lift-to-drag (L/D) ratios than other hypersonic airframe configurations. In addition, flow along the compression surface is contained by the bow shock wave at the leading edges of the vehicle, thereby eliminating crossflow at the engine inlet station. As presented in this article, another benefit of an appropriately designed waverider is the flow uniformity it produces at the engine inlet. The waverider also allows for an inverse design approach since it is generated from a known flowfield. In other words, knowing the engine requirements, a waverider forebody can be developed specifically to produce the required flowfield properties. High L/D ratios, engine inlet flowfield uniformity, no crossflow, and the inverse design capability, combine to make the waverider a promising candidate for an airbreathing hypersonic cruise aircraft. For an accelerator vehicle such as a single-stage-to-orbit or the first stage of a two-stage-to-orbit vehicle, engine inlet flowfield uniformity, no crossflow, and the inverse design capability, make the waverider a promising forebody configuration.

The waverider lends itself well to an optimization process since the on-design aerodynamic forces can be determined relatively quickly, resulting in fairly short single-iteration computational time. To maintain a reasonable single-iteration time, the scramjet combustor is modeled with quasi-one-dimensional flow and the nozzle is modeled with frozen two-dimensional flow. Therefore, the overall flow properties of the engine are represented while still enabling the optimization of the waverider/scramjet as a whole. With this type of code the vehicle configuration with the greatest thrust margin or combination of thrust margin and L/D ratio is determined. The corresponding forebody shape, inlet shape, engine location along the length of the vehicle, engine span, and vehicle volume, are among the properties provided by the optimization. In addition, the approximate thrust margin, L/D, and center of pressure for the optimized configuration, are determined.

Parameters Affecting Integration

A successfully integrated engine/airframe system must yield a high-thrust margin for an accelerator vehicle, a high L/D for a cruise vehicle, and also high-volume efficiency, and low-trim drag by balancing the forebody and nozzle forces. There is an inherent tradeoff between maximizing the thrust margin and maximizing the L/D in an air-breathing hypersonic vehicle with forebody compression and aftbody expansion. The initial expansion angle and area of the nozzle upper wall, in particular, have a significant effect on the relative magnitudes of thrust margin and L/D.

The overall performance of an air-breathing hypersonic vehicle is also affected by the uniformity of the flowfield entering the combustor. Uniform mass flux, pressure, and temperature are essential for effective combustion to occur. Since the vehicle forebody forms the flowfield provided to the engine, this forebody flowfield itself must be uniform, both spanwise and along the height of the inlet. Flow uniformity is one of the benefits of the waverider forebody.

For effective combustion to occur in a reasonable length combustor, pressures between 25–101 kPa (0.25–1 atm), and temperatures between 1000–2000 K (1800–3600°R) must be provided to the combustor entrance. Properties outside these ranges would result in either excessive ignition times or excessive reaction times (if reaction occurs at all), both of which would require an impractical combustor length.[4,5] It is also of interest to shape the inlet to accommodate identical engine modules spanwise across the undersurface of the vehicle. This allows the development and testing of a single engine module, reducing development time and cost.

To maximize the thrust margin the entire airstream between the vehicle undersurface and shock is utilized for mass flow into the engine at the on-design condition. The engine mass flow is governed by the engine span and the shock-layer thickness. The shock-layer thickness varies with engine location along the length of the vehicle.

Presented as Paper 91-1693 at the AIAA 22nd Fluid and Plasmadynamics Conference, Honolulu, HI, June 24–26, 1991; received July 25, 1991; revision received Jan. 3, 1992; accepted for publication Jan. 6, 1992.

*Minta-Martin Fellow, Department of Aerospace Engineering. Student Member AIAA.

†Assistant Professor, Department of Aerospace Engineering. Member AIAA.

In combination with inlet design, flight altitude plays a dominant role in establishing the thermodynamic properties at the combustor entrance. To maintain the entrance temperature and pressure within the ranges previously discussed, there is an altitude ceiling and floor. The altitude ceiling corresponds to the maximum allowable combustor entrance temperature of 2000 K (3600°R) and the minimum allowable entrance pressure of 25 kPa (0.25 atm).[4]

Engine/Airframe Integration Model

Waverider Forebody

The waverider and scramjet are developed as one system in this study. The shape of the waverider forebody is determined by the inlet requirements as follows. For an axisymmetric generating flowfield, the cross-sectional shape of the waverider's bow shock is a circular arc. To maximize the mass capture of the engine (which is particularly important for an accelerator-type vehicle) the cowl lip of the engine must lie as close as possible to the shock, resulting in a circular arc-shaped cowl lip. For identical engine modules to be used spanwise across the majority of the vehicle undersurface, the ideal shape of the vehicle undersurface curve at the inlet station is a circular arc with the same center of curvature as the shock (as shown in Fig. 1). Therefore, the forebody undersurface is formed by streamlines traced forward from the known inlet curve to the bow shock. The upper surface is formed by freestream streamlines traced rearward from the undersurface streamline/shock intersection.

The vehicle shape that results from a circular arc inlet curve is shown at the top of Fig. 2. Although the inlet height is uniform, the resulting forebody configuration is probably not a reasonable design for a vehicle due to aerodynamic heating and volume efficiency considerations. However, if the uniform height restriction is relaxed by making the inlet curve slightly elliptic, the forebody configurations in the center and bottom of Fig. 2 result. For the forebody in the center of the figure, the inlet height at the vehicle center line is 2% greater than that at the most-outboard station. Note the resulting spatulate-shaped configuration. The forebody at the bottom of the figure has an inlet centerline height that is 10% greater than that at the most-outboard station. Thus, a small compromise in the inlet height uniformity leads to a substantial change in the forebody shape.

The inlet curves used in this study are composed of a section of an ellipse (which is centered at the shock circle) and a second-order polynomial that connects the elliptic section to the circular shock. Four parameters govern the shape of the inlet curve as shown in Fig. 3: 1) semiminor ellipse axis; 2) semimajor ellipse axis; 3) percent of the inlet curve span comprised of the ellipse; and 4) the span of the inlet curve.

Since the waveriders are generated from a conical flowfield (which is contained by the leading edges of the waverider) the spanwise variation of flowfield properties at the inlet is only affected by the slight variations in module height. The vertical variations in properties, controlled by the variation in flow between a conical surface and shock, are small. Figure 4 shows a contour plot of the inlet associated with the forebody shown at the bottom of Fig. 2. The pressure variation with height is 8.5% and the mass flux variation is 5%.

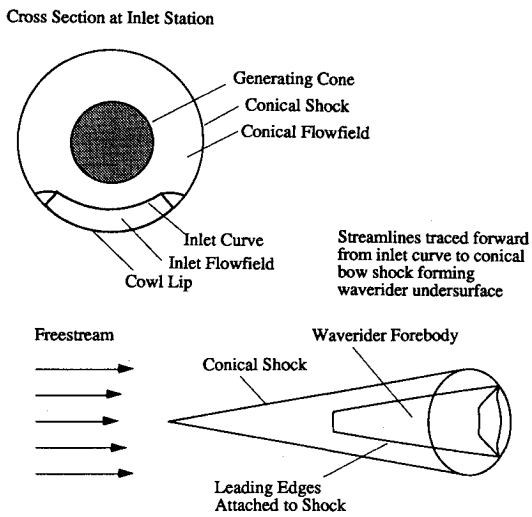

Fig. 1 Waverider forebody construction from circular-arc inlet curve.

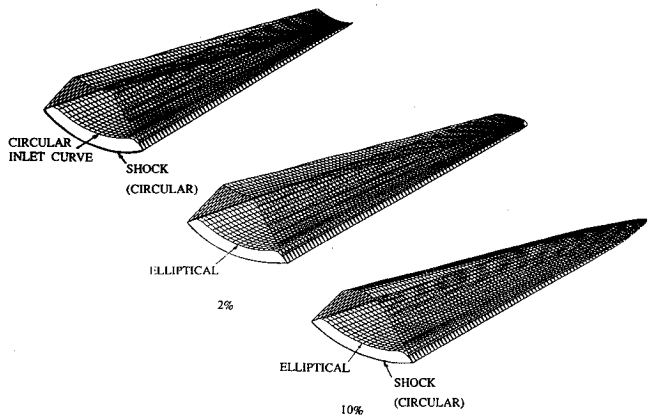

Fig. 2 Waverider forebody configurations derived from circular and elliptic inlet curves, $M = 10$ and $\beta = 15$. Top: circular arc. Center: inlet height 2% greater at vehicle center line. Bottom: inlet height 10% greater at vehicle center line.

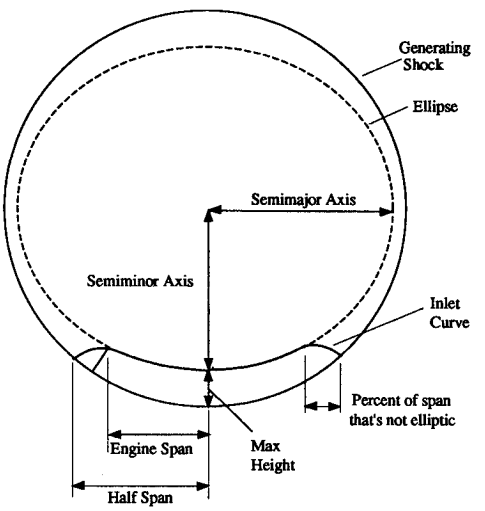

Fig. 3 Optimization parameters.

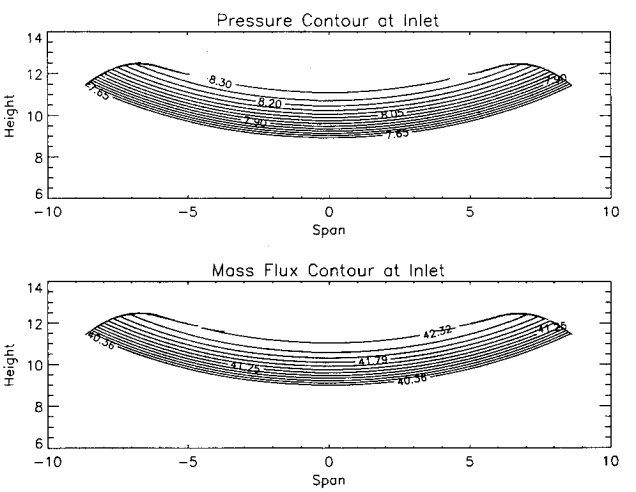

Fig. 4 Contours of pressure (top) and mass flux (bottom) at inlet station, $M = 10$ and $\beta = 15$.

Inlet

The inlet design chosen for this study, is shown in Fig. 5. The cowl surface is formed by streamlines traced from the conical flowfield. The inlet flow is approximated as a two-dimensional planar flow where mass-averaged values of the thermodynamic variables, Mach number, and flow angle are determined from the known properties at the waverider forebody inlet station. These values and $\gamma = 1.4$ are used to determine the ramp shock and reflected shock strength required to achieve the given required combustor entrance temperature as discussed previously. The ramp location is set so that the shock generated by the ramp intersects and reflects off the cowl lip. The reflected shock is required to cancel on the upper wall of the inlet at the combustor entrance while turning the flow back to the angle of the cowl. Once the inlet angles are determined to yield the combustor entrance temperature, the flight altitude is determined by the minimum combustor pressure requirement.

Scramjet/Combustor

Quasi-one-dimensional equations based on those in Shapiro[6] which include area variation, heat addition, friction, mass injection, variation in molecular weight, and ratio of specific heats, are used to analyze the flowfield through the combustor of one engine module. The equations are solved step-by-step from the combustor entrance to the exit using a fourth-order Runge-Kutta technique.

The combustor area variation is designed so that constant pressure combustion occurs. Eliminating or reducing adverse pressure gradients substantially reduces the heat transfer to the combustor walls[7] and avoids flow separation problems. Minimizing the combustor heat transfer is particularly important since the combustor accounts for a substantial amount of the total vehicle heat load.

The rate of combustion and, therefore, the combustor length, are dependent on both the rate of mixing and the rate of reaction. For the set of optimized vehicles presented in this article, a combustor entrance pressure of 25 kPa (0.25 atm) and entrance temperature of 1400 K (2520°R) were used. At these conditions the reaction time given by[8]

$$\tau_R = 325p^{-1.6} \exp(-0.8T_0/1000)$$

where τ_R = reaction time after ignition in μs, p = pressure in atm, and T_0 = initial temperature in K, is great enough that the reaction cannot be assumed to occur instantaneously once complete mixing has occurred. Therefore, both reaction rate and mixing rate must be accounted for in determining the heat release schedule and combustor length. For example, for flight at $M = 10$ and a combustor entrance pressure of 25 kPa (0.25 atm), the combustor length required for reaction time alone is approximately 2.8 m (9.2 ft). At $M = 12$ and 25 kPa (0.25 atm) combustor entrance pressure, the combustor length for reaction time alone is approximately 3.5 m (11.5 ft).

The mixing rate in this study is based on a mixing efficiency derived from experimental results of cold flow mixing with perpendicular injection.[9,10] The mixing efficiency is given as[11]

$$\eta = 1 - e^{-ax}$$

where a = a constant dependent on flow and injector design, and x = distance along combustor in centimeters, and η represents the amount of stoichiometric molecular mixing which has occurred so that no further mixing is required for reaction.

The molecular weight and ratio of specific heats entering the combustor are taken to be those of air at standard conditions. The final values are based on the equilibrium composition of the H_2O-air mixture combusted at the given initial conditions.[12] The variation between the initial and final values is matched to the variation in heat release. Perpendicular fuel injection at an equivalence ratio of one is used for this set of optimized configurations. The total heat released is based on complete combustion from the initial conditions.[12] The reference temperature method is used to estimate the skin friction and wall heat transfer in the combustor.[13]

The starting conditions and geometry of the experimental scramjet combustor tests of Billig[14] were duplicated in the quasi-one-dimensional combustor model to establish the validity of the model. Pressure variation along the combustor correlated reasonably well as shown in Fig. 6 and the total heat transfer predicted by the model was within 8.5% of the experimental data.[4]

Figure 7 shows the heat release distribution and the resultant area variation for a combustor designed for Mach 10 flight. Fuel is added over the first 5% of combustor length by many equally spaced perpendicular injectors.

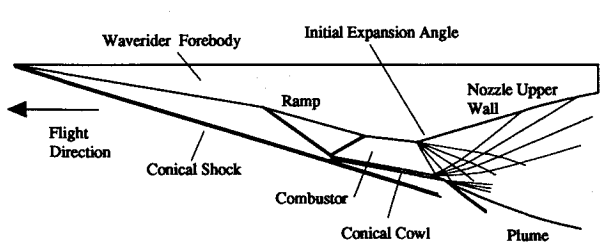

Fig. 5 Inlet ramp and nozzle configuration.

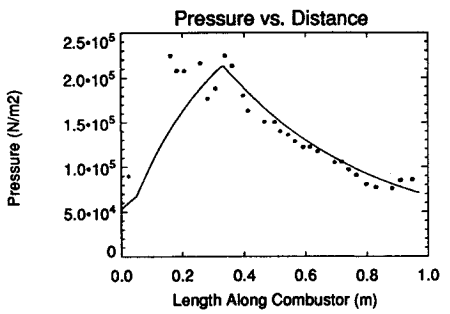

Fig. 6 Pressure comparison along length of combustor. • Experimental data. —Model.

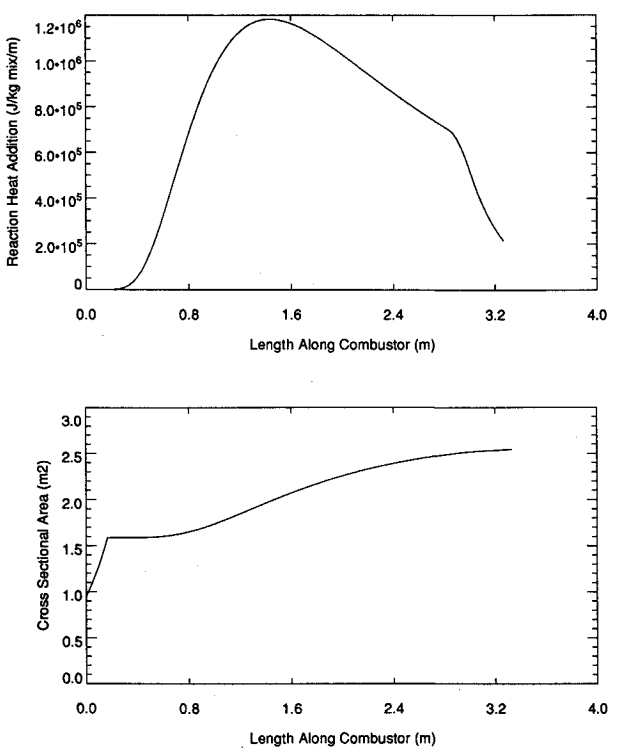

Fig. 7 Combustor heat release distribution and resulting area variation for constant pressure combustion for Mach 10 flight. Combustor entrance conditions are 25 kPa (0.25 atm) and 1400 K (2520°R).

Nozzle

The flowfield through the nozzle is assumed to be frozen at the composition exiting the combustor. The nozzle is then designed for isentropic flow using the two-dimensional planar method of characteristics (see Fig. 5).

A maximum initial upper-wall angle for a given nozzle length is used to maximize the thrust margin. This upper-wall angle is held constant across the span of the nozzle in this study.

The cowl is extended into the nozzle flowfield just far enough so that the cowl chamber intersects the first characteristic emanating from the upper wall. This maintains the highest pressure on the cowl. It also keeps the intersection of characteristics emanating from the cowl with the upper wall farther downstream.[15] This cowl length, therefore, adds to the thrust but still minimizes the total nozzle weight.

The characteristics emanating from the cowl chamfer are those affecting the shape of the nozzle upper wall. Since the exit height of the nozzle is affected by both the upper-wall angle and the characteristics, an iterative process is used to maximize the height. The upper-wall contour is repeated spanwise across the combustor exit to establish the nozzle surface. This analysis is reasonable provided that characteristics reflected from the nozzle plume do not intersect the nozzle upper wall and that the three-dimensional effects in the nozzle are of second order.

Optimization

Five parameters, illustrated in Fig. 3, were allowed to vary in the optimization of the waverider/scramjet system. Four parameters describe the inlet curve shape: 1) semiminor axis of ellipse; 2) semimajor axis of ellipse; 3) percent of inlet curve span comprised of an ellipse; and 4) inlet curve span. The fifth parameter, uniformity of engine height, determines the span of the engine for a given inlet curve.

The system was optimized with $(T - D)/D$ as the objective function in most cases. L/D was also used as an objective function for a constrained forebody length.

The values of L/D and $(T - D)/D$ for a highly integrated vehicle are dependent, in part, on how the forces are accounted for. Figure 8 shows the control volume used for the force calculations. In this work, all vertical forces and the vertical component of engine momentum are added for lift. To calculate the drag, all viscous drag forces are included, but only the drag direction pressure forces are included. An exception is the base drag force which is added into the total drag for the L/D calculation. Base drag is approximated assuming freestream pressure acting on the base area. The resulting L/D and $(T - D)/D$ values reported in this article may be low for the following reason. The control volume of the force calculation is drawn so that the inside forward surface of the cowl is included up to the end of the ramp and the start of the combustor. The negative lift on this surface is added into the lift for L/D, but the thrust on the surface is not subtracted from the drag in either the L/D or the $(T - D)/D$.

The zero-order nonlinear simplex method by Nelder and Mead[16] was used to optimize the system. The optimization in this case is started with six configurations. After the objective function is evaluated for each of the configurations, the configurations are ordered from best to worst. A new configuration is then generated based on the five best configurations. The new configuration then replaces the worst configuration. This optimization technique has been used successfully in previous waverider work.[1,2,17]

An example of the six initial inlet curves is shown in Fig. 9. Also shown on the same figure is the resulting optimized inlet curve. In this case, the objective function was the negative of the thrust margin. Approximately 50 iterations were required before almost no change in the objective function was seen, which is representative of all runs.

One of the benefits of the simplex method for this particular problem is that it explores a large area of the design space by starting with several different initial shapes. This has appeared to decrease the chances of falling into a local minimum when compared to an optimization scheme, such as Conmin,[18] which uses the method of steepest descent from only one initial shape.

Results

Conically derived 62 m (203 ft) waveriders integrated with scramjet engines were optimized at flight Mach numbers of 10 and 12 at several generating shock or bow shock angles β. The primary objective function chosen for this study was thrust margin. Figure 10 shows the variation of the maximized thrust margin with a generating shock angle at Mach 10 and Mach 12 for the optimized configurations. Thrust margin decreases with increasing generating shock angle, and also decreases with increasing Mach number. Also shown in Fig. 10, L/D increases with Mach number, but the values of L/D for a vehicle maximized for thrust margin are low. As discussed above, if the thrust from the forward cowl inside-surface is included in the L/D and thrust-margin calculation, these values are greater by approximately 30% for all configurations.

As generating shock angle increases the vehicle volume, planform area and height of the optimized configuration increases. As shown in Fig. 11, drag increases substantially with increasing volume. The lowest vehicle volume for each flight Mach number in Fig. 11 corresponds to the $\beta = 10$ shock angle and the highest vehicle volume corresponds to the $\beta = 16$ shock angle. The increase in volume and resultant increase in drag help to explain why the thrust margin decreases with

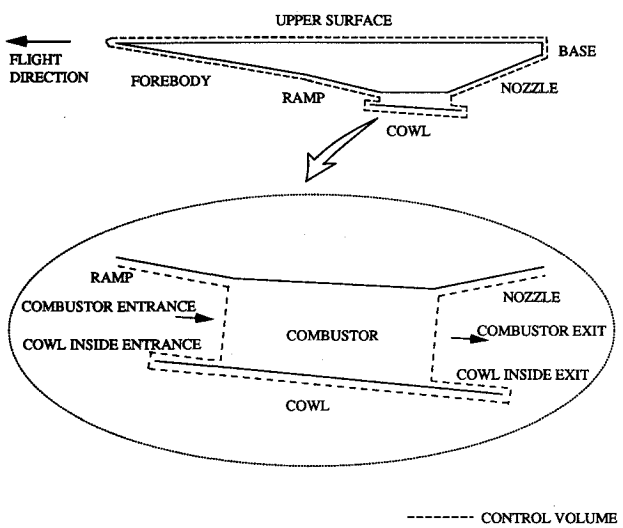

Fig. 8 Control volume for force calculation.

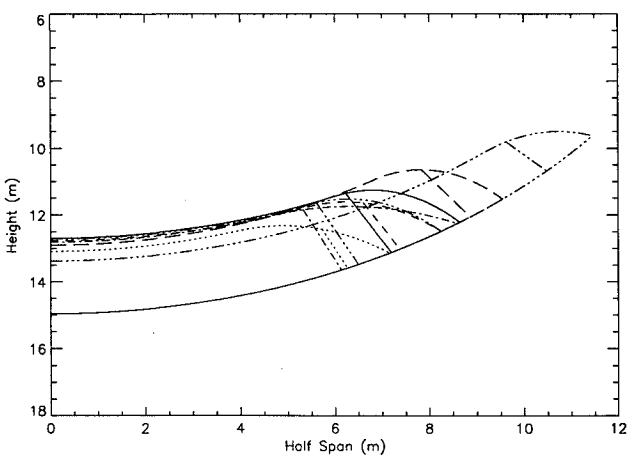

Fig. 9 Initial and optimized inlet curves. Solid line is optimized curve.

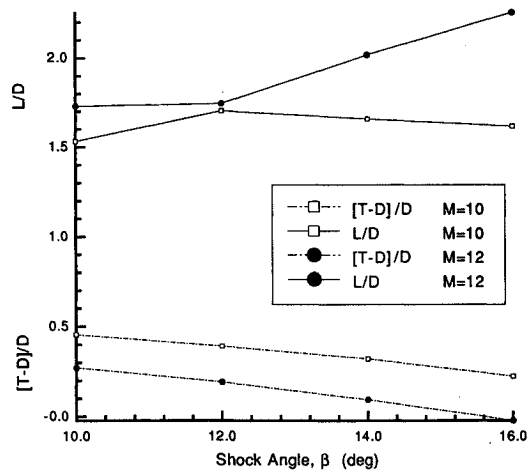

Fig. 10 Variation of thrust margin and L/D ratio with generating shock angle for Mach 10 and Mach 12 configurations optimized for thrust margin.

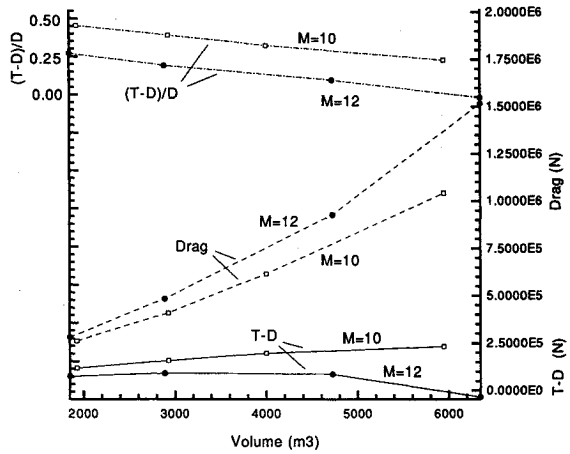

Fig. 11 Variation of thrust margin $(T - D)/D$, and absolute thrust margin $T - D$, and drag with volume for Mach 10 and Mach 12 configurations optimized for thrust margin.

shock angle. In addition, Fig. 11 shows the variation of absolute thrust margin, $T - D$, with vehicle volume. Absolute thrust margin increases slowly (slower than the increase in drag) with volume for the Mach 10 vehicles for the range of volumes calculated. For the Mach 12 vehicles, absolute thrust margin increases and then decreases with volume. Note that the $\beta = 16$ Mach 12 vehicle has such a high drag that the thrust margin is no longer positive.

The increase in vehicle drag with volume results from both wave drag and friction drag. Wave drag or pressure drag accounts for 71–82% of the total drag for the Mach 12 vehicles. The percentage increases from the low to the high value with increasing volume. For the Mach 10 vehicles, wave drag ranges from 76 to 85% of the total drag.

Figures 12–15 show the lift and drag distributions on the Mach 12, $\beta = 10$ and $\beta = 14$ shock-angle vehicles. The bar labeled "Forebody" includes the undersurface forward of the ramp and the complete upper freestream surface. "Outboard" refers to the section of the undersurface outboard of the engine and downstream from the start of the ramp. "Interior Cowl" includes the inside surface of the cowl upstream of the combustor and the inside surface downstream of the combustor. "Nozzle" includes the upper wall and side walls of the nozzle. "Engine" is the momentum change through the combustor. Note that the lift from the nozzle, even for a configuration optimized for thrust margin, is significant compared to the sum of forebody, outboard, ramp, and exterior cowl lift. Note also the large magnitude of the ramp drag. The ramp forces are for the entire ramp, including the section

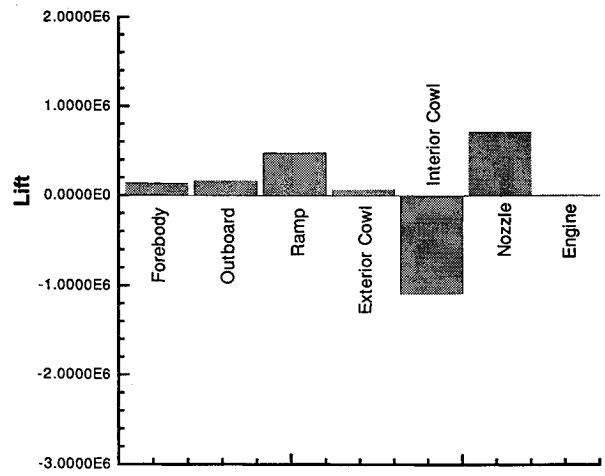

Fig. 12 Lift distribution on Mach 12 waverider with a 10-deg shock angle.

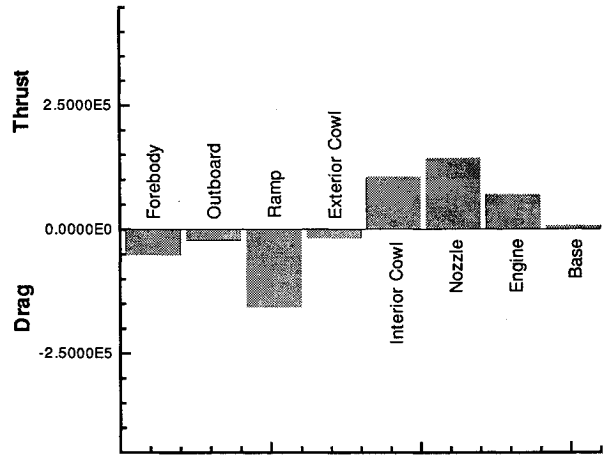

Fig. 13 Drag/thrust distribution on Mach 12 waverider with a 10-deg shock angle.

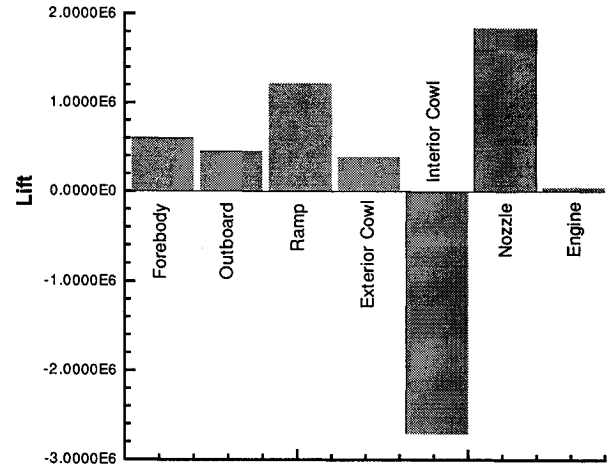

Fig. 14 Lift distribution on Mach 12 waverider with a 14-deg shock angle.

that extends past the cowl lip to the entrance of the combustor. The percentage of the total cowl interior force that acts upstream of the combustor is between 42–49% for all configurations. Therefore, the ramp drag and interior forward cowl thrust counteract each other. The same is true for the ramp and interior forward cowl lift. The nozzle, engine, and inside exit surface of the cowl all contribute significantly to the thrust. For all optimized configurations the nozzle flow is substantially underexpanded.

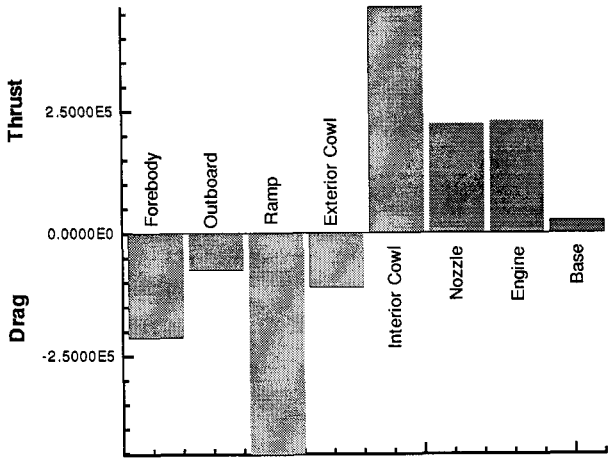

Fig. 15 Drag/thrust distribution on Mach 12 waverider with a 14-deg shock angle.

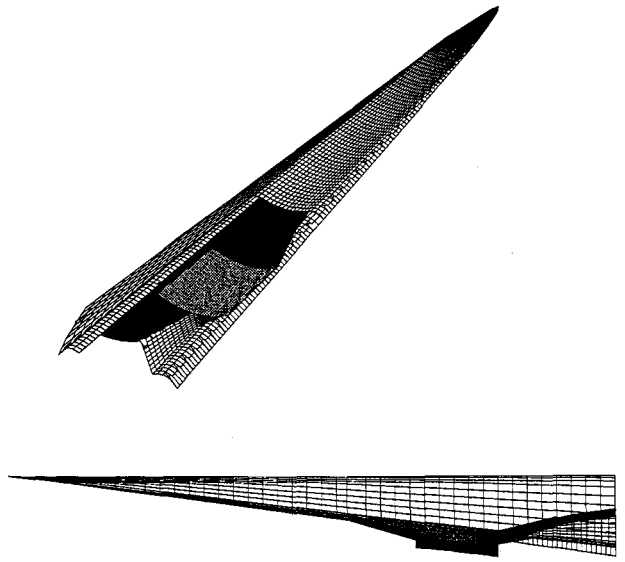

Fig. 16 Mach 12, β = 10 scramjet integrated waverider optimized for $(T - D)/D$.

Perspective and side views of these two configurations are shown in Figs. 16 and 17. The β = 10 configuration is much more slender and shorter in height than the β = 14 configuration, causing the lower forces shown in the previous figures. The engine location is further aft for the β = 10 configuration and the cowl for this configuration is significantly shorter than for the β = 14 configuration. The center of pressure is 67% of the vehicle length from the nose, or 0.24 m (0.8 ft) behind the cowl lip for the β = 10 configuration, and 63% of the vehicle length from the nose, or 1.3 m (4.3 ft) behind the cowl lip for the β = 14 configuration.

The optimization was also run with L/D as the objective function. When the engine location was unconstrained, the optimizer drove the engine forward along the vehicle length resulting in a nozzle length approximately 20 m (66 ft) longer than that for vehicles optimized for thrust margin. This is an expected result since the pressure and, therefore, lift forces are greater on the nozzle than on the remainder of the vehicle. Also, the value of L/D for the nozzle alone is greater than for the other components. The thrust margin for this configuration was 0.076 and decreasing, and the L/D was 4.5 before the optimization was stopped.

To achieve a high L/D and reasonable thrust margin, tighter constraints were placed on the minimum forebody length, or equivalently the maximum nozzle length. The optimization was then run again for maximum L/D. Figure 18 shows the resulting perspective and side view for the Mach 10, β = 14

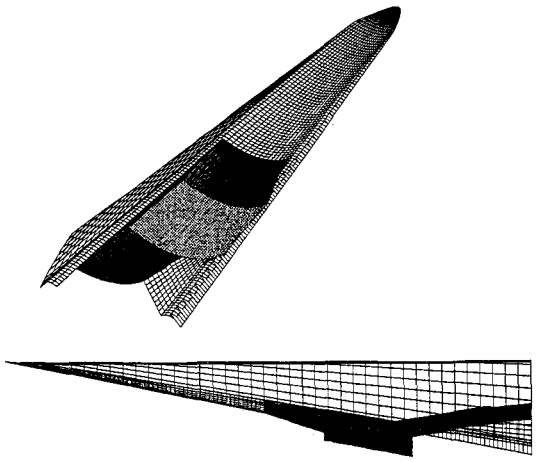

Fig. 17 Mach 12, β = 14 scramjet integrated waverider optimized for $(T - D)/D$.

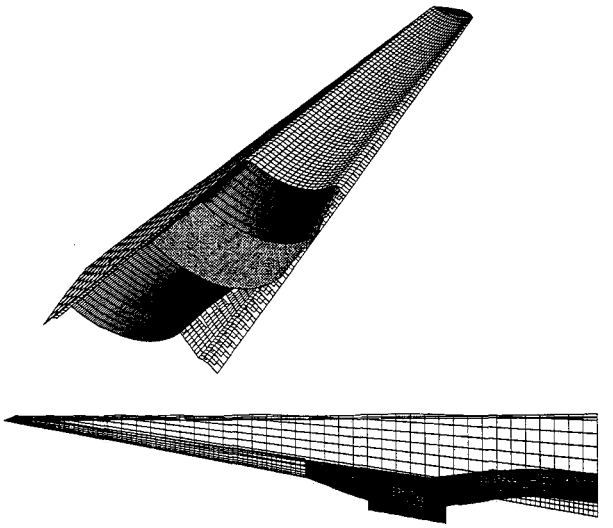

Fig. 18 Mach 10, β = 14 scramjet integrated waverider optimized for L/D with constrained forebody length.

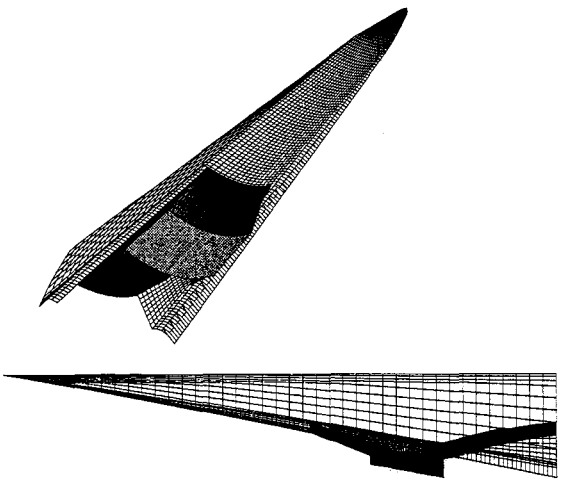

Fig. 19 Mach 10, β = 14 scramjet integrated waverider optimized for $(T - D)/D$.

configuration optimized for L/D with the forebody length constraint. For this configuration, L/D = 2.90, $(T - D)/D$ = 0.140, vehicle volume = 5219 m^3 (184,300 ft^3), and the center of pressure is 72% of the vehicle length from the nose, or 6.8 m (22 ft) behind the cowl lip. Note the bluntness of the nose. The bluntness is caused by a more circular-shaped inlet curve which also causes a slightly concave upper surface. As a comparison, Fig. 19 shows the perspective and side view

for the Mach 10, $\beta = 14$ configuration optimized for thrust margin. Note that the engine is located further aft on this vehicle. Also, this configuration is smaller in span but greater in thickness than the vehicle optimized for L/D. For this configuration L/D = 1.65, $(T - D)/D = 0.321$, vehicle volume = 4000 m^3 (141,300 ft^3), and the center of pressure is 65% of the vehicle length from the nose, or 0.46 m (1.5 ft) ahead of the cowl lip.

Figures 20–23 show the lift and drag force distributions of the vehicle optimized for L/D and thrust margin, respectively. The nozzle force is more in the lift direction for the configuration optimized for L/D, and more in the flight direction for the thrust-margin optimized vehicle (as expected from comparing the side views of the configurations).

For the constrained L/D optimization, the nozzle exit height was set at the maximum value. Nozzle exit height is the height of the nozzle upper wall at the exit plane at the vehicle centerline above the upper wall expansion angle. This contributed to maintaining a reasonable value for thrust margin. When the nozzle exit height was allowed to vary in the optimization, further increases in L/D resulted, but thrust margin degraded. For the $M = 10$, $\beta = 14$ configuration and the same constrained L/D optimization (except with the addition of the nozzle exit height as an optimization parameter) the optimized results were L/D = 3.41 and $(T - D)/D = 0.023$. The nozzle exit height was approximately 1.2 m (3.9 ft) or 33% less than the maximum for this case. The resulting thrust margin is worse than allowing the engine to move farther forward along the vehicle as in the unconstrained L/D optimization. As for both previous L/D optimized vehicles, this configuration has

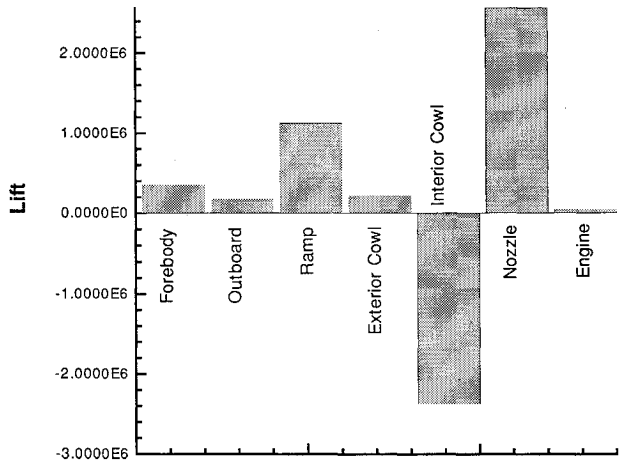

Fig. 20 Lift distribution on Mach 10 waverider with a 14-deg shock angle, optimized for L/D with constrained forebody length.

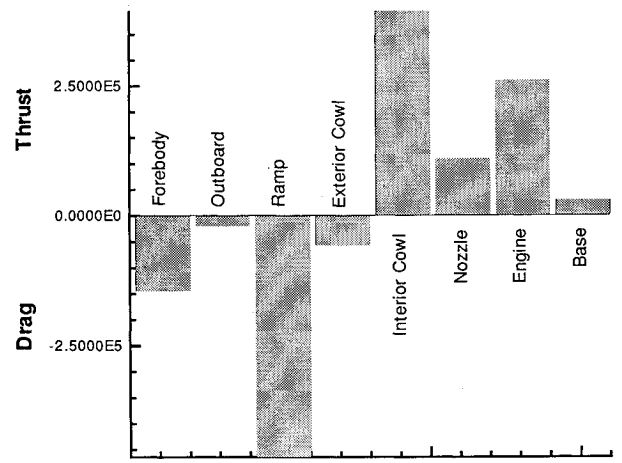

Fig. 21 Drag/thrust distribution on Mach 10 waverider with a 14-deg shock angle, optimized for L/D with constrained forebody length.

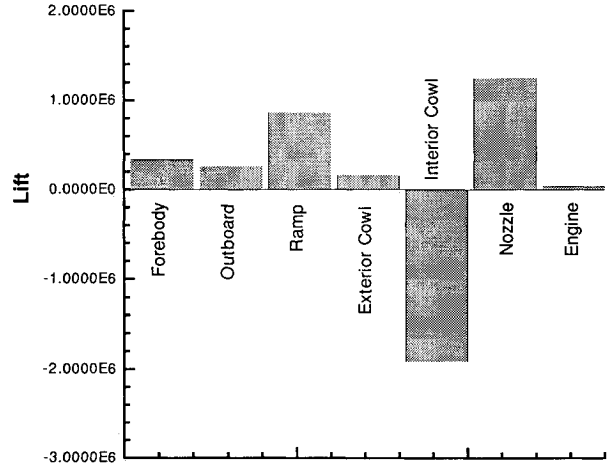

Fig. 22 Lift distribution on Mach 10 waverider with a 14-deg shock angle, optimized for thrust margin.

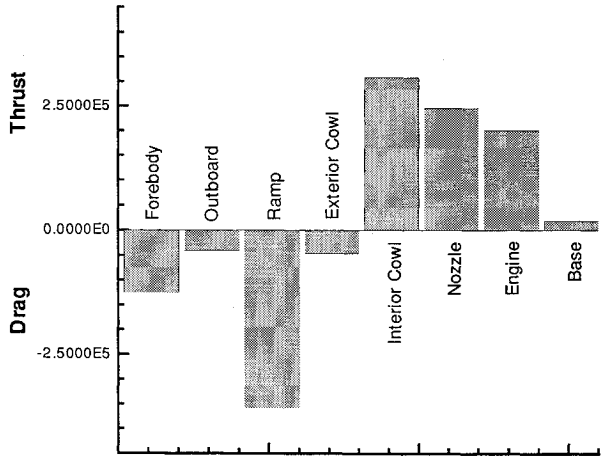

Fig. 23 Drag/thrust distribution on Mach 10 waverider with a 14-deg shock angle, optimized for thrust margin.

a blunt nose with a forward engine, but the vehicle span is not as great. For this vehicle, volume = 4612 m^3 (162,900 ft^3) and the center of pressure (c.p.) was 70% of the vehicle length from the nose, or 7.9 m (26 ft) behind the cowl lip. The total drag for both vehicles optimized for L/D is less than that for vehicles of equivalent volume, but optimized for thrust margin. This is expected since the nozzle makes up a larger percentage of the vehicle and does not add to wave drag. The ratio of wave drag to total drag for both L/D optimized vehicles is a few percent less than that for the thrust-margin optimized vehicle.

All c.p. values are given with power-on. Power-off will result in lower pressures in the combustor and on the inside cowl exit and nozzle surfaces. For these configurations, the loss in lift on the nozzle will have the predominant effect, causing the c.p. of the vehicle to move forward.

All of the vehicles were optimized with a conically derived cowl and a combustor entrance pressure of 25 kPa (0.25 atm) and entrance temperature of 1400 K (2520°R). For the Mach 10 and Mach 12 waveriders this resulted in altitudes between 39–42 km (128,000–138,000 ft). Inlet contraction ratios (freestream height divided by combustor entrance height at the vehicle centerline) for all cases varied between 18–27, generally increasing with decreasing generating shock angle. The flight altitude for 25 kPa (0.25 atm) and 2000 K (3600°R) combustor entrance conditions is approximately 47 km (154,000 ft). This corresponds to the maximum flight altitude for effective combustion.

All of the computations were done on a Sun4 computer. One optimization with 100 iterations takes approximately 1000 s of cpu time to complete.

Conclusions

The configurations presented are examples of the first scramjet/integrated optimized waveriders. The waverider is an excellent configuration for scramjet engine integration for the following reasons: 1) uniform properties, both spanwise and along the inlet height, are provided by a waverider forebody; 2) no crossflow occurs at the inlet at the on-design point; 3) the waverider produces a high L/D, important for cruise vehicles; and 4) an inverse design approach is possible, whereby the known flowfield and geometry requirements of the engine lead to the appropriate vehicle configuration. The combined waverider and quasi-one-dimensional scramjet model lends itself readily to the development and optimization of the scramjet/waverider system due to relatively short single iteration computation times.

Thrust margin and L/D are highly coupled in these integrated vehicles. The combination of thrust margin and L/D for a vehicle will be set by the application and mission. For vehicles optimized for thrust margin, thrust margin decreases with increasing shock angle due to higher vehicle volumes and higher resultant drag. Increasing vehicle volume by 1000 m^3, for vehicles between 2000 and 6000 m^3 in volume and 62 m in length, results in a 5.8% decrease in thrust margin for Mach 10 vehicles and a 6.5% decrease in thrust margin for Mach 12 vehicles. Thrust margin also decreases with increasing Mach number. Optimized vehicles at Mach 12 have thrust margins that are approximately 0.2 less than those at Mach 10 for all vehicle volumes in the range considered. For a vehicle volume of approximately 2900 m^3 this results in a 50% decrease in thrust margin for the Mach 12 vehicle compared to the Mach 10 vehicle. Optimizing for L/D causes the engine to move forward, increasing the nozzle planform area. At Mach 10, optimizing for L/D increases the L/D ratio by 75% and decreases the thrust margin by 50% relative to a thrust margin optimized vehicle of the same 5200 m^3 volume.

Inlets with small variations in height with span result in promising vehicle forebody configurations. In addition, combustor entrance pressure and temperature requirements limit the maximum flight altitude for any inlet design.

Future Work

Future work will include optimizing the configurations with an objective function of (L/D)*Isp for greater cruise range. For the objective functions in the current study and in future work, nozzles with initial expansion angles which vary with span will be considered. Also nozzle side walls will be allowed to decrease in size. In addition, the axial location on the generating shock wave of the cowl lip itself will be allowed to vary. The effect of this would be to allow a variation in the spanwise radius of curvature of the cowl lip for a given generating shock angle. Finally, other flight Mach numbers and other combustor entrance conditions within the required range will be investigated.

Acknowledgments

The authors acknowledge the Minta Martin Foundation at the University of Maryland and the Zonta International Foundation for financial support in the form of fellowships, and Isaiah Blankson of the NASA Generic Hypersonics Program for support and encouragement.

References

[1]Bowcutt, K. G., Anderson, J. D., and Capriotti, D., "The Viscous Optimize Hypersonic Waveriders," AIAA Paper 87-0272, Reno, NV, Jan. 1988.

[2]Corda, S., and Anderson, J. D., Jr., "Viscous Optimized Waveriders Designed From Axisymmetric Flowfields," AIAA Paper 88-0369, Reno, NV, Jan. 1988.

[3]Bauer, S., "Analysis of Two Viscous Optimized Waveriders," First International Hypersonic Waverider Symposium, Univ. of Maryland, College Park, MD, Oct. 1990.

[4]O'Neill, M. K. L., and Lewis, M. J., "Scramjet Integration on a Waverider," First International Hypersonic Waverider Symposium, Univ. of Maryland, College Park, MD, Oct. 1990.

[5]Biasca, R. J., "Chemical Kinetics of Scramjet Propulsion," M.S. Thesis, Dept. of Aeronautics and Astronautics, Massachusetts Inst. of Technology, MA, Sept. 1988.

[6]Shapiro, A. H., *The Dynamics and Thermodynamics of Compressible Fluid Flow*, Vol. 1, Wiley, New York, 1953, pp. 219–226.

[7]Pinckney, S. Z., "Turbulent Heat Transfer Prediction Method for Application to Scramjet Engines," NASA TN D-7810, Nov. 1974.

[8]Rogers, R. C., and Schexnayder, C. J., Jr., "Chemical Kinetic Analysis of Hydrogen-Air Ignition and Reaction Times," NASA TP 1856, July 1981.

[9]Rogers, R. C., "Mixing of Hydrogen Injected from Multiple Injectors Normal to a Supersonic Airstream," NASA TN D-6476, Sept. 1971.

[10]Anderson, G. Y., and Gooderum, P. B., "Exploratory Tests of Two Strut Fuel Injectors for Supersonic Combustion," NASA TN D-7581, Feb. 1974.

[11]Jachimowski, C. J., "An Analytical Study of the Hydrogen-Air Reaction Mechanism With Application to Scramjet Combustion," NASA TP-2791, 1988.

[12]Drell, I. L., and Belles, F. E., "Survey of Hydrogen Combustion Properties," NACA Rept. 1383, 1957.

[13]Eckert, E. R. G., "Engineering Relations for Heat Transfer and Friction in High-Velocity Laminar and Turbulent Boundary-Layer Flow Over Surfaces with Constant Pressure and Temperature," *Transactions of the American Society of Mechanical Engineers*, Vol. 78, No. 6, 1956, pp. 1273–1283.

[14]Billig, F. S., and Grenleski, S. E., "Heat Transfer in Supersonic Combustion Processes," *Fourth International Heat Transfer Conference*, Elsevier, Amsterdam, Aug. 1971.

[15]Small, W. J., Weidner, J. P., and Johnston, P. J., "Scramjet Nozzle Design and Analysis as Applied to a Highly Integrated Hypersonic Research Airplane," NASA TN D-8334, Nov. 1976.

[16]Nelder, J. A., and Mead, R., "A Simplex Method for Function Minimization," *Computer Journal*, Vol. 7, Jan. 1965, pp. 308–313.

[17]McLaughlin, T. A., *Viscous Optimized Hypersonic Waveriders for Chemical Equilibrium Flow*, M.S. Thesis, Dept. of Aerospace Engineering, Univ. of Maryland, College Park, MD, 1990.

[18]Vanderplaats, G. N., and Moses, F., "Structural Optimization by Methods of Feasible Directions," *Journal of Computers and Structures*, Vol. 3, July 1973, pp. 739–755.